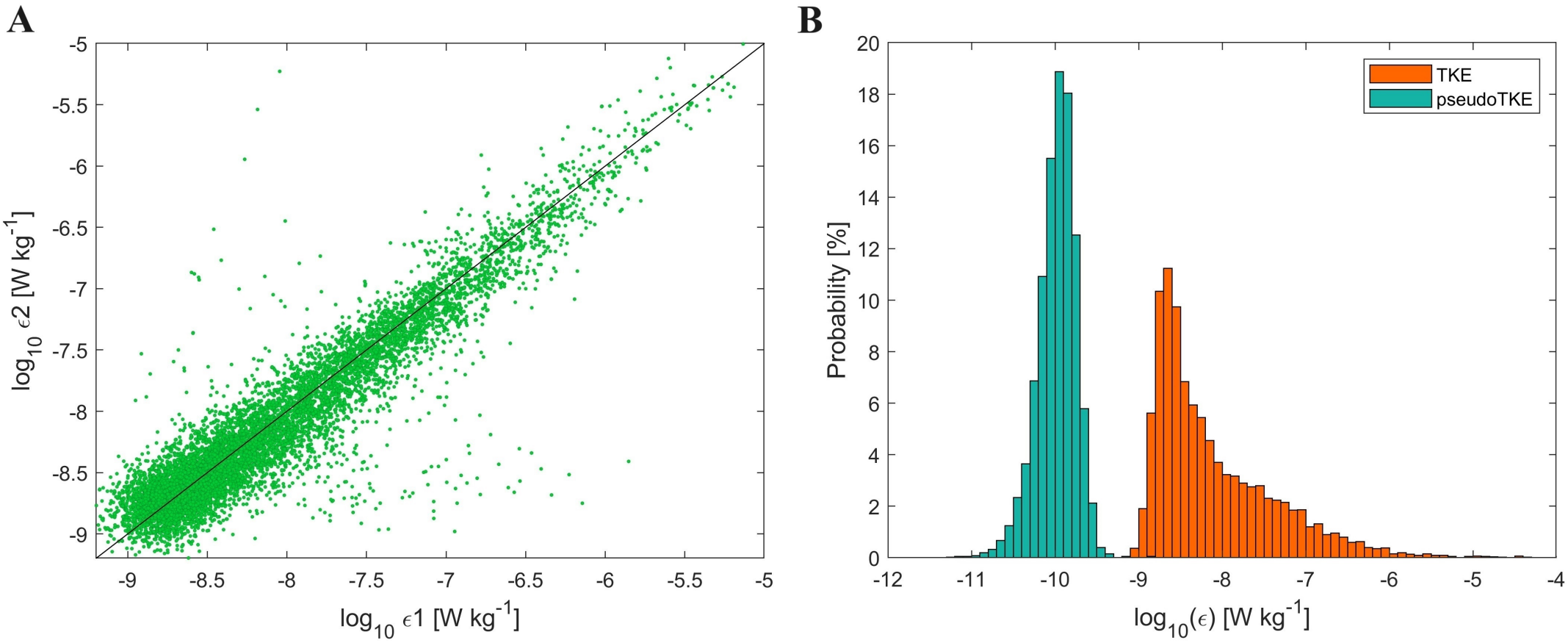

Supplementary Figure 1. Turbulent dissipation rates (ε1 and ε2) recorded from both shear sensors (**A**) and probability distribution frequency for turbulent kinetic energy dissipation rates and pseudo dissipation rates **(B)**. The black solid line in panel (**A**) represents the 1:1 proportion between ε1 and ε2.

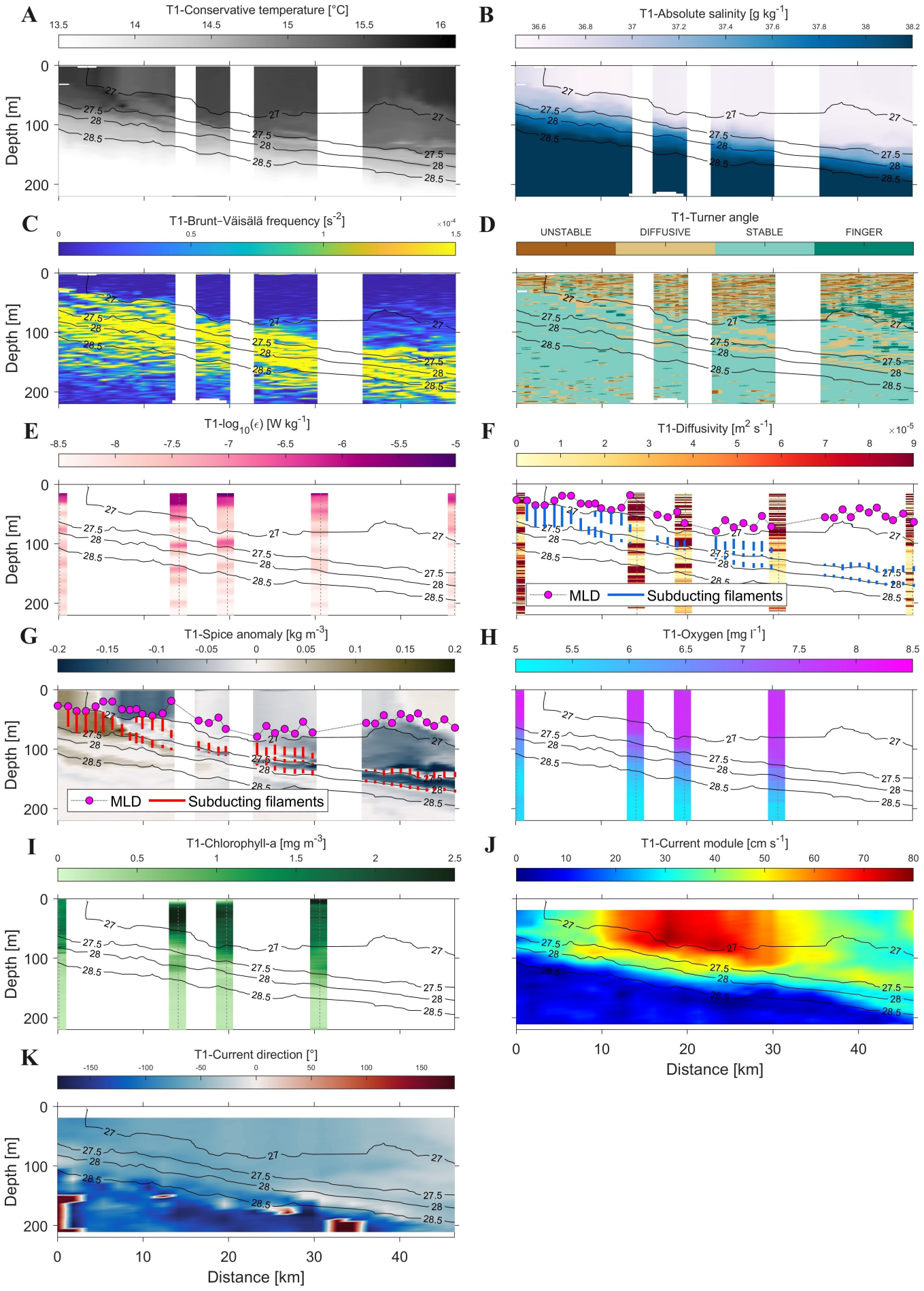

Supplementary Figure 2. Absolute temperature **(A)**, conservative salinity **(B)**, Brunt–Väisälä frequency **(C)**, Turner angle **(D)**, turbulent kinetic energy dissipation rates **(E)**, diffusivity **(F)**, spice anomaly **(G)**, dissolved oxygen **(H)**, chlorophyll-a **(I)**, current module **(J)** and direction **(K)** estimations along the transect 1 of the 2019 CALYSPSO campaign. Black lines represent the density anomaly isopycnals, whereas the grey dashed lines indicate the microstructure sampling stations location. The distance between stations was calculated starting from the sampling point located to the east.

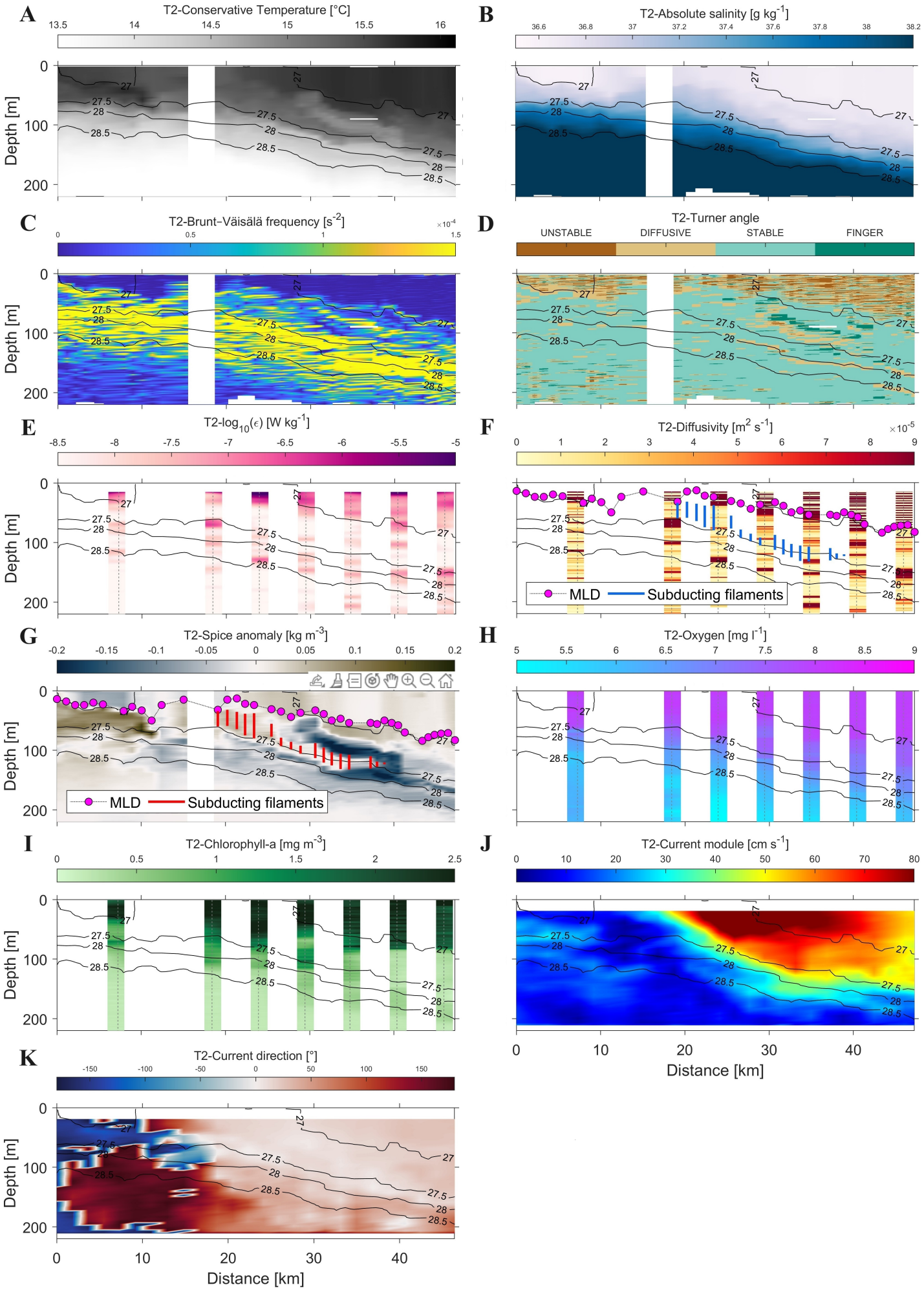

Supplementary Figure 3. Same as Supplementary Figure 2 but for transect 2 of the 2019 CALYPSO campaign. The distance between stations was calculated starting from the sampling point located to the north.

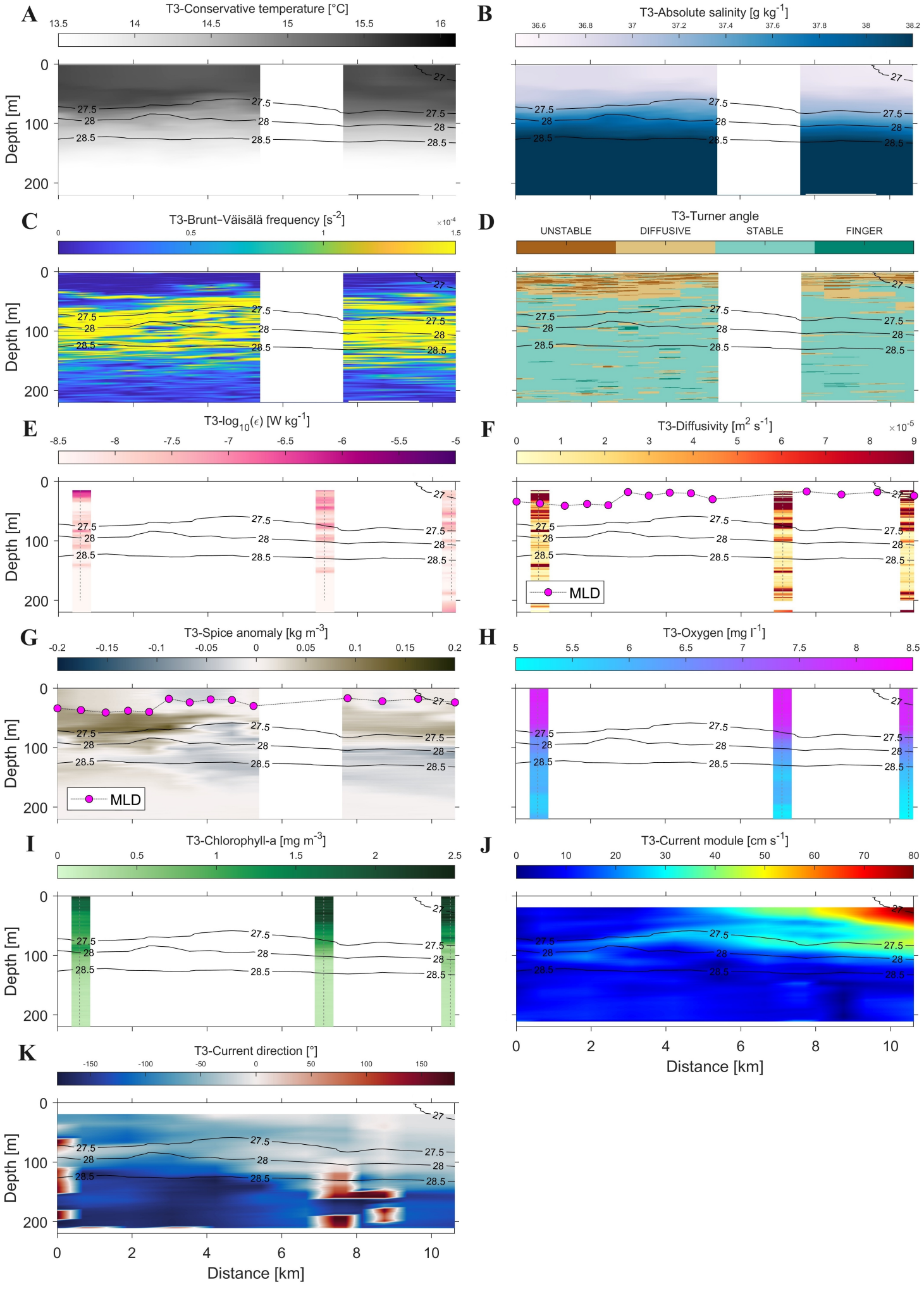

Supplementary Figure 4. Same as Supplementary Figure 3 but for transect 3 of the 2019 CALYPSO campaign.

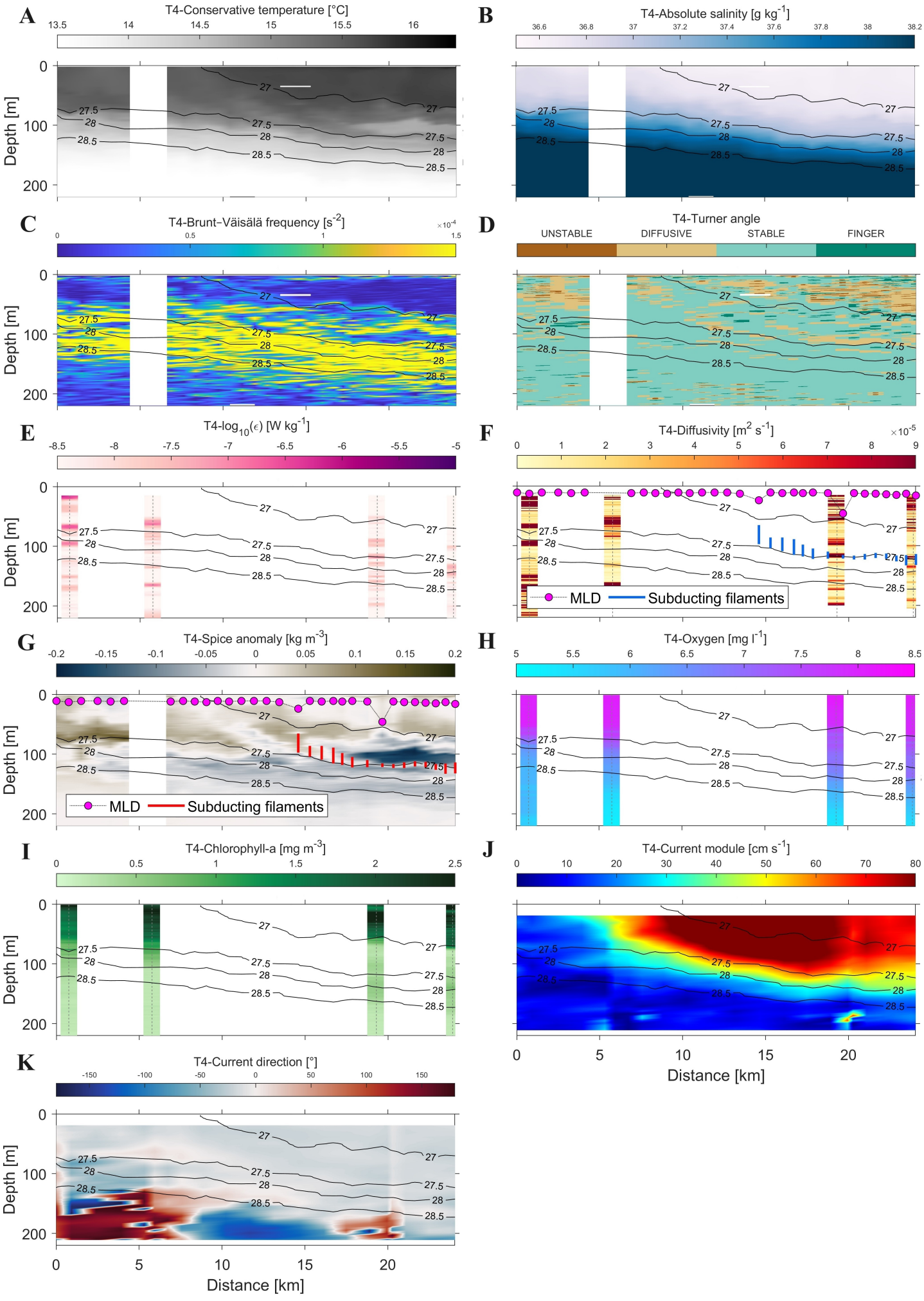

Supplementary Figure 5. Same as Supplementary Figure 3 but for transect 4 of the 2019 CALYPSO campaign.

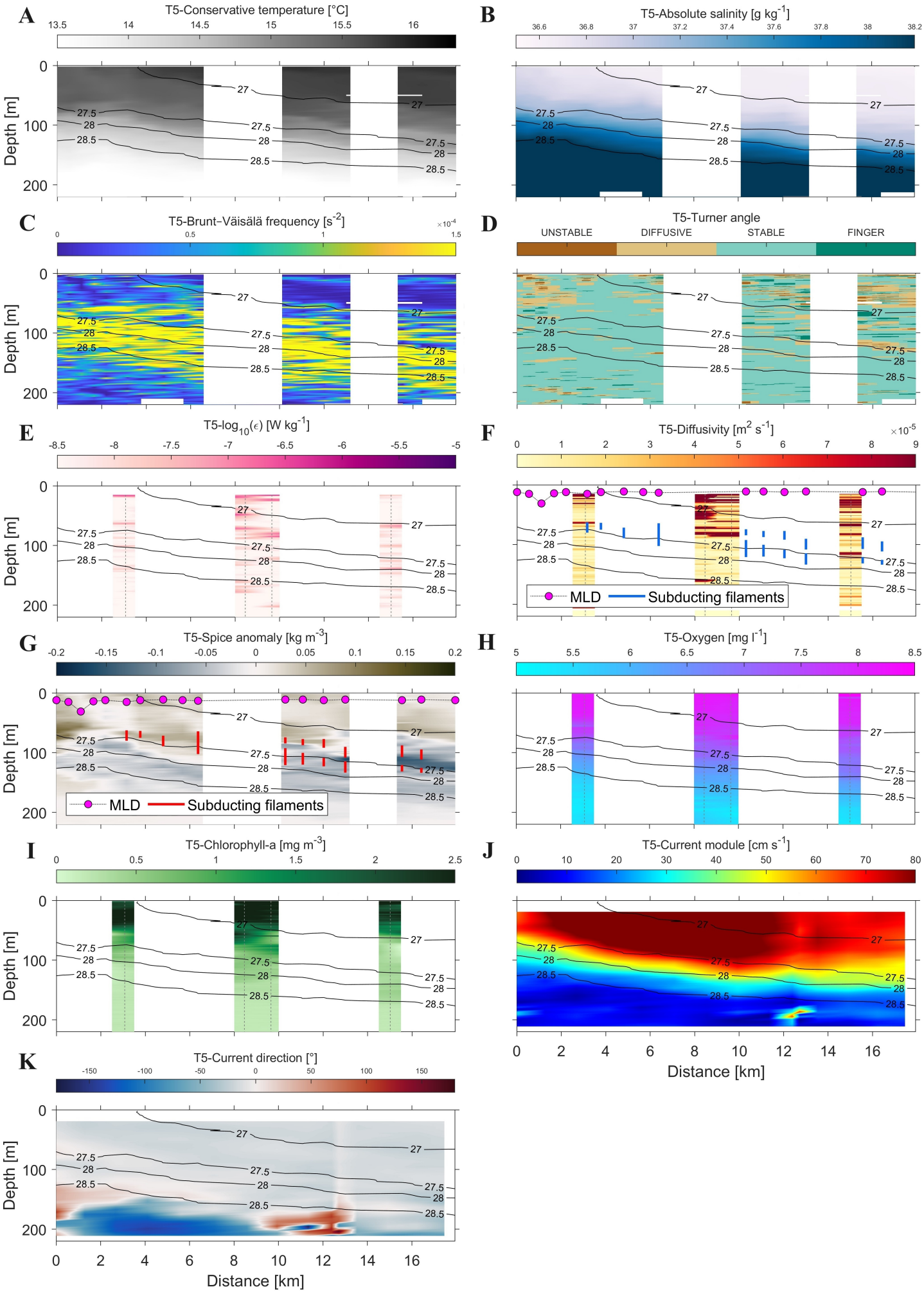

Supplementary Figure 6. Same as Supplementary Figure 3 but for transect 5 of the 2019 CALYPSO campaign.

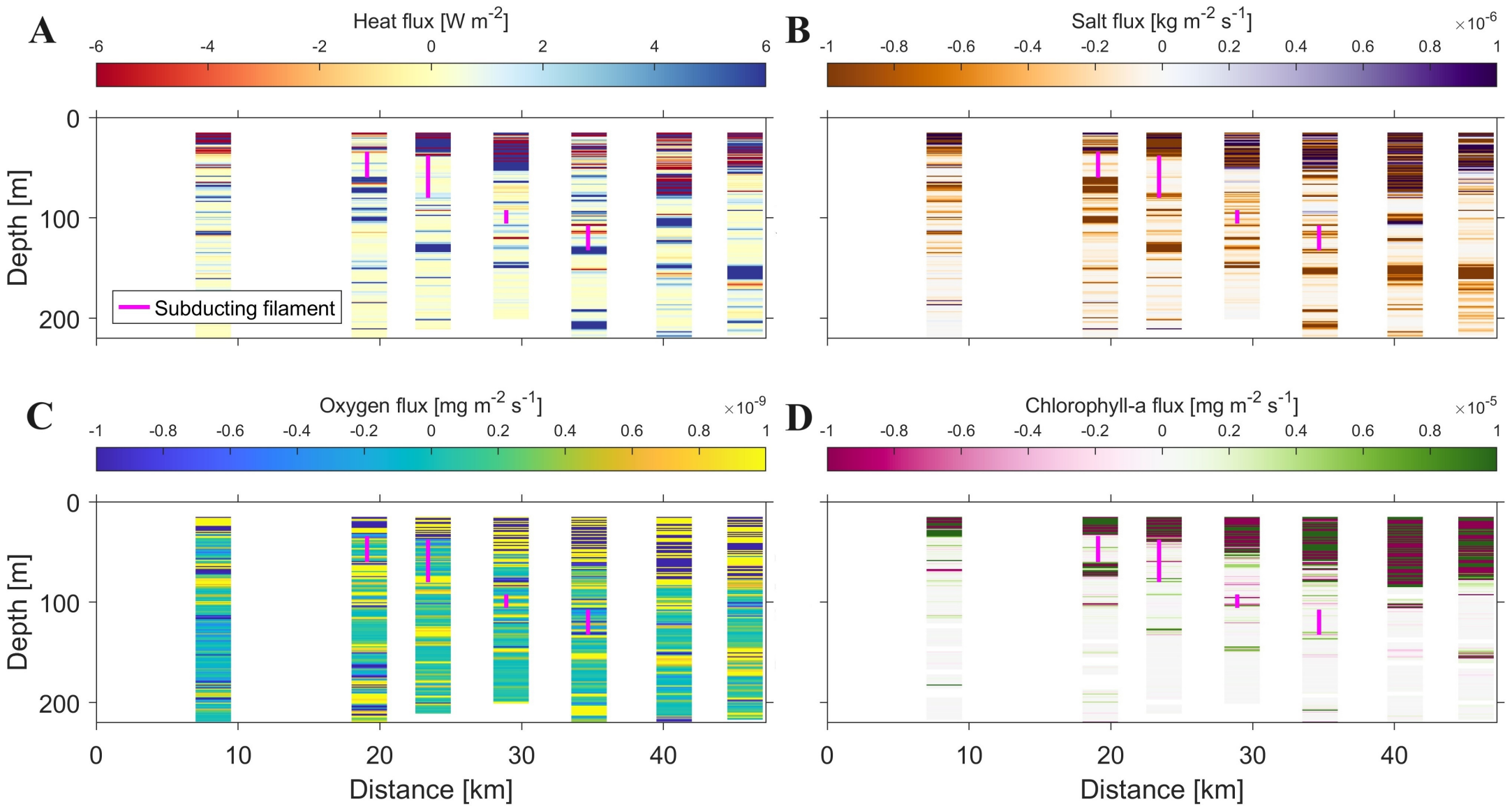

Supplementary Figure 7. Heat **(A)**, salt **(B)**, dissolved oxygen **(C)** and chlorophyll-a **(D)** turbulent fluxes estimated during four profiles of transect 2.

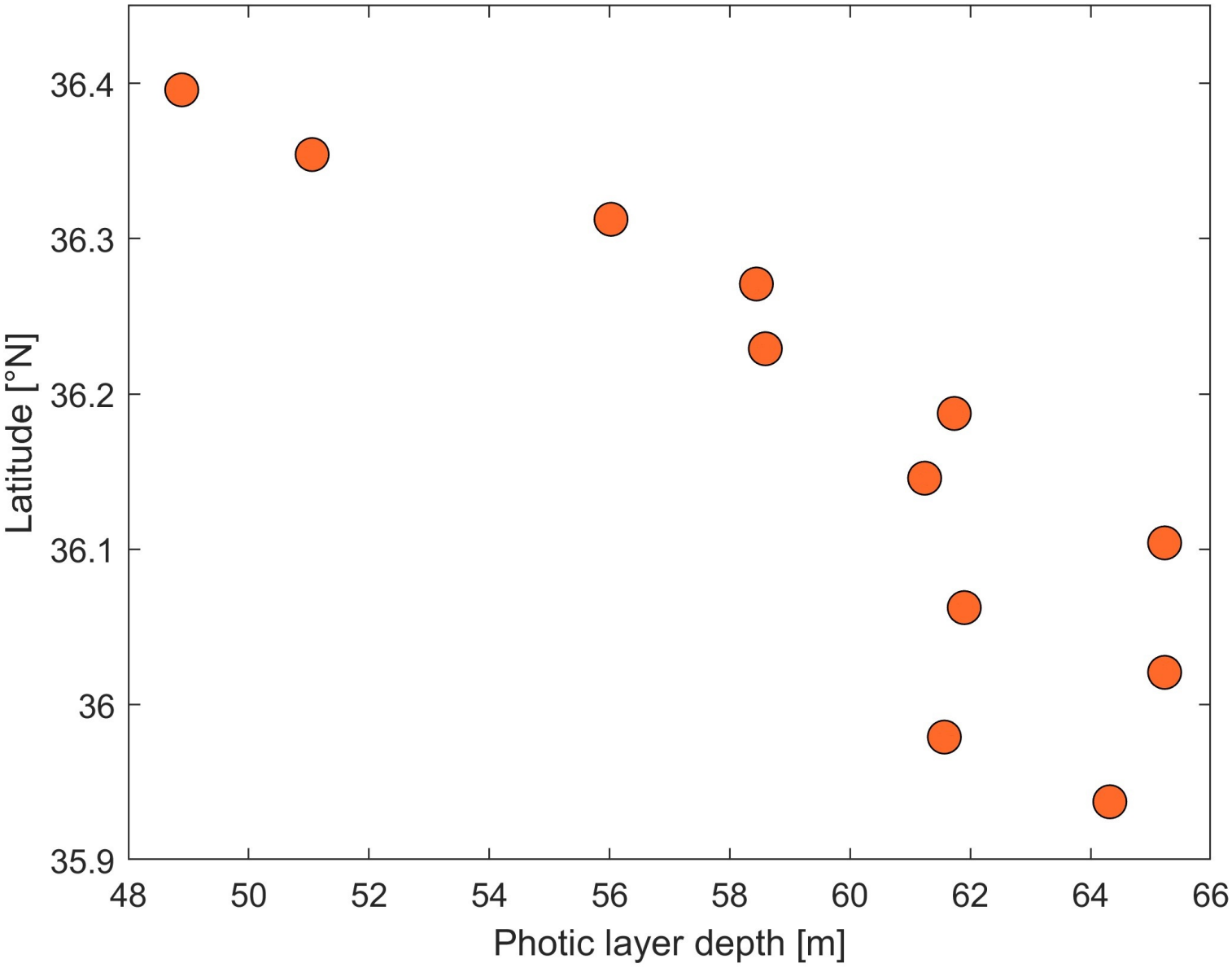

Supplementary Figure 8. Satellite-derived photic layer depth variability along transect 2 of 2019 CALYPSO campaign. The meridional variability of the monthly composite (16th March-16th April 2019) at 4.1°W longitude is shown. Photic layer depth estimations (spatial resolution: 4 km) were computed from the diffuse attenuation coefficient data collected during the Aqua Moderate Resolution Imagining Spectroradiometer (MODIS) mission and following Behrenfeld *et al.* (2005; https://doi.org/10.1029/2004GB002299).

Supplementary Table 1. Uncertainties assessment of turbulent fluxes of heat, salt, oxygen and chlorophyll-a along the upper and lower boundaries of the subducting intrusion identified within transect T2 of the 2019 CALYPSO campaign (refer to Table 2 for additional details). The relative contributions of diffusivity (Kz) and the vertical variable gradient ($\partial X/\partial z$) to the total flux uncertainty are expressed as percentages.

Distance	**Boundary**	**Heat flux**	**k_z**	**$\partial T/\partial z$**	**Salt flux**	**k_z**	**$\partial S/\partial z$**	**O_2 flux**	**k_z**	**$\partial O_2/\partial z$**	**Chl flux**	**k_z**	**$\partial Chl/\partial z$**
[km]		[W m^{-2}]	[%]	[%]	[kg m^{-2} s^{-1}]	[%]	[%]	[mg m^{-2} s^{-1}]	[%]	[%]	[mg m^{-2} s^{-1}]	[%]	[%]
0													
	Upper	22.8	98.9	1.1	$5.0\cdot10^{-7}$	98.7	1.3	$3.9\cdot10^{-9}$	81.3	18.7	$2.0\cdot10^{-5}$	94.4	5.6
	Lower	25.8	90.1	9.9	$2.6\cdot10^{-7}$	88. 4	11.6	$4.5\cdot10^{-9}$	55.9	44.1	$9.9\cdot10^{-6}$	74.7	25.3
4.3													
	Upper	4.7	76.3	23.7	$2.0\cdot10^{-7}$	95.8	4.2	$2.6\cdot10^{-9}$	74.1	25.9	$1.6\cdot10^{-5}$	84.0	16.0
	Lower	2.3	97.2	2.8	$1.8\cdot10^{-8}$	89. 5	10.5	$1.5\cdot10^{-9}$	88.0	12.0	$1.9\cdot10^{-6}$	80.6	19.4
9.8													
	Upper	0.9	78.7	21.3	$1.6\cdot10^{-8}$	93.2	6.8	$3.1\cdot10^{-10}$	14.3	85.7	$7.1\cdot10^{-7}$	27.6	72.4
	Lower	1.2	98.0	2.0	$7.7\cdot10^{-9}$	92.0	8.0	$2.2\cdot10^{-10}$	36.4	63.6	$7.0\cdot10^{-7}$	22.3	77.7
15.6													
	Upper	1.3	84.7	15.3	$1.3\cdot10^{-8}$	84.9	15. 1	$4.2\cdot10^{-10}$	1.7	98.3	$2.9\cdot10^{-7}$	1.5	98.5
	Lower	6.9	78.5	21.5	$1.7\cdot10^{-8}$	37.2	62.8	$2.0\cdot10^{-9}$	82.5	17.5	$8.3\cdot10^{-7}$	18.8	81.2

The uncertainty associated with turbulent was assessed by employing error propagation methods outlined in Taylor (1997). The standard deviation of each parameter involved in equations (5), (6) and (7) was utilized in this analysis. Furthermore, the propagation error calculation facilitates the assessment of the distinct contributions of various sources of uncertainty to the overall uncertainty. This information is crucial, as a heightened proportion of uncertainty attributed to diffusivity may signify an ambiguity in flux magnitude, while uncertainty primarily arising from variable vertical gradients may suggest uncertainty in flux sign determination.

Taylor, R.J., 1997. An Introduction to Error Analysis: The Study of Uncertainties in Physical Measurements. 2nd Ed., University Science Books

Supplementary Table 2. Estimations of daily turbulent (Turb) and convective diffusive (Diff) heat, salt, oxygen and chlorophyll-a fluxes, calculated at four stations along the subducting intrusion within transect 2 of the 2019 CALYPSO campaign. Negative (positive) values denote a loss (gain) within the interior of the intrusion. Please note that diffusive convection fluxes were computed exclusively for the upper intrusion boundary, as these conditions were met only in that specific region. The effective diffusivity of heat and salt caused by diffusive convection was estimated following Nakano and Yoshida (2019) and Nagai et al. (2021).

Distance	**Heat flux** [°C]		**Salt flux** [g kg^{-1}]		**O_2 flux** [mg l^{-1}]		**Chl flux** [mg m^{-3}]	
[km]	Turb	Diff	Turb	Diff	Turb	Diff	Turb	Diff
0	$-2.2\cdot10^{-2}$	$-5.4\cdot10^{-5}$	$5.1\cdot10^{-3}$	$-3.5\cdot10^{-6}$	$-5.5\cdot10^{-3}$	$3.5\cdot10^{-5}$	$-3.4\cdot10^{-3}$	$1.9\cdot10^{-4}$
4.3	$-2.9\cdot10^{-3}$	$-1.4\cdot10^{-5}$	$-9.1\cdot10^{-3}$	$-2.0\cdot10^{-6}$	$-6.9\cdot10^{-3}$	$-3.1\cdot10^{-5}$	$-2.9\cdot10^{-2}$	$-2.0\cdot10^{-4}$
9.8	$-4.4\cdot10^{-3}$	$-1.4\cdot10^{-4}$	$-7.6\cdot10^{-4}$	$-1.3\cdot10^{-5}$	$-6.7\cdot10^{-4}$	$8.1\cdot10^{-5}$	$-6.2\cdot10^{-3}$	$-2.5\cdot10^{-4}$
15.6	$-1.1\cdot10^{-2}$	$-8.4\cdot10^{-4}$	$7.0\cdot10^{-4}$	$-7.8\cdot10^{-5}$	$-1.1\cdot10^{-2}$	$1.7\cdot10^{-4}$	$-2.2\cdot10^{-3}$	$1.1\cdot10^{-4}$

The effective diffusivity of heat caused by diffusive convection was estimated following equation (S1) from Nakano and Yoshida (2019) and Nagai et al. (2021):

$$K_\theta = 0.909\,\nu \exp\left[4.6 \exp\left(-0.54({R_\rho}^{-1} - 1)\right)\right] \qquad \text{(S1)}$$

where R_ρ represents the density ratio $R_\rho = \left(\alpha \frac{\partial T}{\partial z}\right)\left(\beta \frac{\partial S}{\partial z}\right)^{-1}$, with α and β denoting the heat and salt expansion coefficients, respectively. Conversely, haline diffusivity (for observed R_ρ<0.5) was computed using equation (S2):

$$K_S = 0.15 R_\rho K_\theta \qquad \text{(S2)}$$

Heat and salt fluxes under conditions of diffusive convection were quantified following equations (5) and (6) with the effective thermal (K_θ) and haline (K_S) diffusivity values, respectively. Moreover, biogeochemical diffusive convection fluxes were estimated using equation (7) in conjunction with the effective thermal diffusivity values, as per Nagai *et al*. (2021).

Nagai, T., Rosales Quintana, G.M., Durán Gómez, G.S., Hashihama, F., Komatsu, K., 2021. Elevated turbulent and double-diffusive nutrient flux in the Kuroshio over the Izu Ridge and in the Kuroshio Extension. J. Oceanogr. 77, 55–74. https://doi.org/10.1007/s10872-020-00582-2

Nakano, H., Yoshida, J., 2019. A note on estimating eddy diffusivity for oceanic double-diffusive convection. J. Oceanogr. https://doi.org/10.1007/s10872-019-00514-9